KeAi
CHINESE ROOTS
GLOBAL IMPACT

Available online at www.sciencedirect.com

ScienceDirect

Green Energy & Environment 6 (2021) 298–307

www.keaipublishing.com/gee

Research paper

Highly efficient energy harvest via external rotating magnetic field for oil based nanofluid direct absorption solar collector

Debing Wang [a,1], Wenwen Liang [a,1], Zhiheng Zheng [a,b,*], Peiyu Jia [a], Yunrui Yan [a], Huaqing Xie [a], Lingling Wang [a,b], Wei Yu [a,c,*]

[a] School of Environmental and Materials Engineering, College of Engineering, Shanghai Polytechnic University, Shanghai, 201209, China
[b] Research Center of Resource Recycling Science and Engineering, Shanghai Polytechnic University, Shanghai, 201209, China
[c] Shanghai Key Laboratory of Engineering Materials Application and Evaluation, College of Engineering, Shanghai Polytechnic University, Shanghai, 201209, China

Received 14 November 2019; revised 17 March 2020; accepted 30 March 2020
Available online 8 April 2020

Abstract

Nanofluids based direct absorption solar collectors (DASCs) are considered as the important alternative for further improve the utilization of solar energy. However the low-quality energy and aggregation of nanoparticles obstructs their large-scale application. In this work, a new method of using magnetic nanofluids in DASCs is proposed. By this method, not only high-quality energy is got as well as the problems of blockage and corrosion in heat exchanger are well avoided. The result shows that the maximum temperature can reach 98 °C under 3 solar irradiations and the photothermal conversion efficiency can be further increased by 12.8% when the concentration is 500 ppm after adding an external rotating magnetic field. The highest viscosity of working fluid reduced by 21% when the concentration is 500 ppm at 95 °C after separating the Fe_3O_4@C nanoparticles from the nanofluids via magnetic separation technology. Meanwhile, the obtained pure base liquids with high temperature flow to heat exchanger, which also reduces the flow resistance in pipeline and avoids the problems such as blockage and corrosion in heat exchanger. This research promotes a new way for the efficient utilization of solar energy.

Keywords: Direct absorption solar collector; Magnetic Fe_3O_4@C-oil nanofluids; Magnetic separation technology; High-quality energy

1. Introduction

As a new and renewable energy, solar energy is rapidly developed in recent years. The research mainly focus on photovoltaics [1], photocatalysis [2], artificial photosynthesis [3] and photothermal conversion [4]. Among them, the solar thermal is considered as the most potential and simplest way of solar application, which has received more and more attention [5,6]. It is generally known that the key problem is how to improve the efficiency of solar collector for this technology. To achieve high photothermal efficiency, the direct absorption solar collectors (DASCs) was proposed by Minardi in the 1970s [7]. In DASCs, the light can be absorbed directly by working fluids and converted into heat. Compared with the traditional solar collectors, it has significantly higher photothermal conversion efficiency and lower heat loss. Based on DASCs, the working fluids are becoming a key factor on the efficiency of solar collector. An efficient working fluid must both exhibit excellent optical absorption properties in broadband wavelengths and have a high thermal conductivity. The high light absorption is favorable for capturing sunlight and high thermal conductivity of working fluids enables rapid

* Corresponding authors.
E-mail addresses: zhiheng_zheng@163.com (Z. Zheng), yuwei@sspu.edu.cn (W. Yu).
[1] Both authors contributed equally to this work and should be considered co-first authors.

https://doi.org/10.1016/j.gee.2020.03.014

thermal transportation throughout the entire collectors and minimizes the heat loss. However, it's hard for conventional working fluids such as ethylene glycol and water to have both all above characteristics.

Along with the nanotechnology development, nanofluids, firstly proposed by Choi in 1995 [8], has brought a new development space for working fluids. Many researchers have found out that the introduction of nanoparticles exerts a positive influence on thermophysical properties of base fluid. Yu et al. prepared the stable ethylene glycol-based copper nanofluids and discussed the effect of copper nanoparticle on thermal conductivity of fluids. They observed a 46% enhancement ratio when the content of copper is 0.5 vol% at 50 °C [9]. And they also investigated the photothermal conversion efficiency of dual plasmonic Au/TiN nanofluids and found that the efficiency was higher than base liquid of EG [10]. Therefore, the nanofluids based DASCs is regarded as a promising solution for capturing solar energy. The typical DASCs with a closed-loop circulating nanofluids is shown in Fig. 1(a) [11]. Until now, although various photothermal nanoparticles including carbon-based nanomaterials [12,13], plasmonic nanoparticles [14,15] and alloy particles [16] have been studied extensively, the large-scale application is restricted due to its two inherently defects. On the one hand, the photothermal conversion efficiency is very sensitive to the concentration of nanofluids. Based on earlier finds, the temperature distribution in the receiver is extremely uneven when the concentration of nanofluids is high [17], which causes the low-quality energy. In addition, nanofluids are thermodynamically unstable systems due to their high surface energy and high specific surface area. Therefore, nanofluids extremely suffer from the aggregation of nanoparticles, which causes some serious problems such as blockage of heat exchanger in practical application [18–20]. On the other hand, compared with the low temperature type (< 80 °C), the literature about the medium-temperature (80−120 °C), a wide variety of applications ranging from building heating, seawater desalination to some industrial heat etc, is relatively little. This is also one of the important factors to restrict its large-scale applications.

To obtain high-quality energy, the key is to explore a suitable heat transfer fluid. Compared with conventional water, the air, heat transfer oil and molten salt are more suitable as high temperature heat transfer fluids due to their high ability of heat absorption and thermal conductivity. Although the operating temperature range of air is also very large, it cannot store heat due to small specific heat capacity. As for molten salt, many excellent thermal properties such as the higher operating temperature and the larger specific heat capacity, has been widely used in heat exchanger system [21,22] and solar power generation [23,24]. However, the antifreezing is always a notable problem in molten salt in winter. All things considered, the heat transfer oil seems to be ideal nanofluids used as the heat transfer fluid, owning its lower system pressure and good operating safety in DASCs. Meanwhile, it has low viscosity and good pumpability [25].

Based on the unique structure and good magnetic property of magnetic nanoparticle [26–28]. In this work, we proposed a new method of using magnetic nanofluids containing Fe_3O_4@C as the working fluids of DASCs. The working mechanism diagram is shown in Fig. 1b. In this method, the high-quality energy is first obtained under 3 sunlight irradiations at external rotating magnetic field which can be well solved the problem of the non-uniform temperature distribution in DASCs [29,30]. Then Fe_3O_4@C nanoparticles are separated from the high temperature nanofluids by magnetic separation technology. The obtained pure base liquids with high temperature flow to heat exchanger where all kinds of high temperature liquids that we needed can be obtained. By this way, not only high-quality energy is got, but also the problems of blockage and corrosion in heat exchanger are well avoided. Thereby it promoted a new way for the efficient utilization of solar energy.

2. Experimental section

Iron chloride hexahydrate ($FeCl_3 \cdot 6H_2O$), sodium dihydrogen phosphate (NaH_2PO_4) and glucose are available from Sinopharm Chemical Reagent Co. Ltd., Shanghai, China. The heat transfer oil (L-QB320) is purchased from Guangzhou Changxin Trade Co., Ltd. All of them are used without further purification.

2.1. Nanofluids synthesis and preparation

Stable Fe_3O_4@C-Oil nanofluids are prepared with different concentrations by a two-step synthetic method. In this method, the magnetic nanoparticles Fe_3O_4@C are firstly

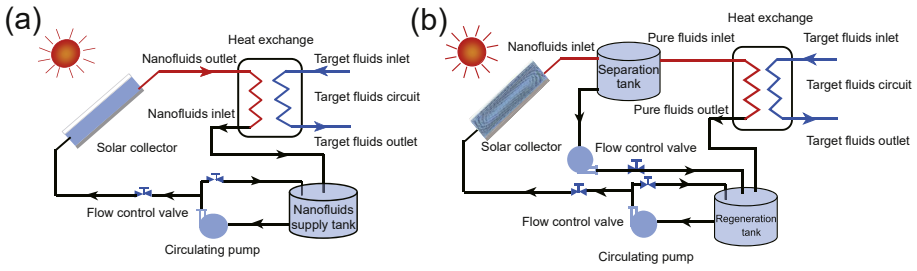

Fig. 1. (a) Typical DASCs with a closed-loop circulating nanofluid. (b) The proposed hypothetical working mechanism model.

synthesized with spindle-like α-Fe_2O_3 as precursor according to the record in literatures [31,32]. Typically, 27.03 g of $FeCl_3 \cdot 6H_2O$ and 0.27 g of NaH_2PO_4 are sonicated in 375 mL of deionized (DI) water for 1 h in a beaker at room-temperature. The obtained suspension is transferred to a 500 mL Teflon autoclave and then heated at 105 °C for 48 h. After the autoclave cools to room temperature, the α-Fe_2O_3 precursors are collected by centrifugal separation, washing with deionized water several times. 3.75 g of α-Fe_2O_3 precursors are sonicated in 62.5 mL of DI water for 30 min in a beaker. In another beaker, 7.5 of glucose is dissolved in 62.5 mL of DI water. Then an aqueous solution of α-Fe_2O_3 and 125 mL of ethanol are added into the glucose suspension. The obtained mixture is transferred to a 500 mL Teflon autoclave and heated at 190 °C for 12 h. Finally, the product is centrifuged and washed with DI water and calcinated at 600 °C for 12 h under nitrogen.

Nanofluids with different concentrations (50, 100, 300, 500 and 500 ppm) are synthesized by dispersing Fe_3O_4@C in oil and then ultrasonic for 30 min.

2.2. Instrumentations

The SEM imaging is performed using a Hitachi (S4800) scanning electron microscope. And the chemical composition of the samples is further investigated by SEM with EDS. The X-ray diffraction (XRD) was carried out with a Bruker D8-Advancer. The magnetic properties of the sample are measured using Vibrating sample magnetometer (VSM, Lake Shore 7307). The viscosity and optical property of the nanofluids are recorded by rheometer (TA Instruments, Ar 2000 Ex) and Ultraviolet−visible−near infrared spectrophotometer (Agilent Cary 5000) at 25 °C, respectively.

2.3. Evaluation of the photothermal conversion properties

A schematic of the photothermal conversion experimental system is described in our previous work [30]. In this research, the radiation intensity and magnetic field intensity are set at 3000 W m^{-2} and 50 mT, respectively. In addition, the total energy and photothermal conversion efficiency of overall system are used to evaluate the photothermal properties of nanofluids. They can be calculated by using following formula (1) and (2) [33]:

$$Q = C_p \sum_{i=1}^{4} (m_i \Delta T_i) \tag{1}$$

$$\eta = \frac{C_p \sum_{i=1}^{4} m_i \Delta T_i}{AG\Delta t} \tag{2}$$

where, Q is the total energy of overall system, m_i and ΔT_i represent the mass of each unit nanofluids and maximum temperature rise in 2500 s irradiation time, C_p is the specific heat capacity of nanofluids. Notably, since the concentration of nanomaterials is low, the mass and specific heat of nanofluids are approximately equal to that of oil. A is the top surface area of nanofluids accepting irradiation (4.0 cm^2). G is the irradiation power on the top surface of nanofluids (3000 W m^{-2}) and Δt is the time exposed to solar radiation.

2.4. Uncertainty analysis in measurements

The total errors of experimental measurements are mainly caused by system (bias) and random (precision). The bias introduced by the system can be neglected because it is usually considered to remain constant during testing. The precision error is determined by formula [34]:

$$u_r^2 = \left(\frac{\partial r}{\partial X_1}\right)^2 u_{X_1}^2 + \left(\frac{\partial r}{\partial X_2}\right)^2 u_{X_2}^2 + \cdots + \left(\frac{\partial r}{\partial X_j}\right)^2 u_{X_j}^2 \tag{3}$$

where U_r and U_{X_i} are the uncertainty of direct measurement result and direct measurement result, respectively.

The photothermal conversion performance for nanofluids is a function of the mass m, the specific heat C_p, the increment of temperature ($T_s - T_i$), irradiation intensity G, the solar incident areas A and irradiation time Δt according to the Eq. (2). Therefore, the uncertainty of the photothermal conversion efficiency can be obtained by the following equation:

$$\frac{U_\eta}{\eta} = \left[\left(\frac{U_m}{m}\right)^2 + \left(\frac{U_{C_p}}{C_p}\right)^2 + \left(\frac{U_{T_s-T_i}}{T_s-T_i}\right)^2 + \left(\frac{U_G}{G}\right)^2 + \left(\frac{U_A}{m_A}\right)^2 + \left(\frac{U_t}{t}\right)^2\right]^{0.5} \tag{4}$$

In our work, solar incident areas A is determined by width d. The measurement of m, C_p, T, d, G, and Δt are respectively: ±0.01 g, ±1%, ±0.1 °C, ±0.01 mm, ±4% and ±0.1 s. Every item could be calculated as flows:

$$\frac{U_m}{m} = \frac{0.01}{100} = 0.01\%, \frac{U_{C_p}}{C_p} \le 1\%, \frac{U_{T_s-T_i}}{T_s-T_i} = \frac{0.1}{73} = 0.137\%, \frac{U_G}{G} = \frac{0.04}{3000} = 0.0013\%,$$

$$\frac{U_{\Delta t}}{\Delta t} = \frac{1}{2500} = 0.04\%, \frac{U_A}{m_A} = \left(2\left(\frac{U_d}{d}\right)^2\right)^{0.5} = \left(2\left(\frac{0.1}{100}\right)^2\right)^{0.5} = 0.14\%$$

The final result is $U_\eta/\eta = 1.02\%$.

3. Results and discussion

3.1. Characterization of materials

Fig. 2a–b shows the SEM image of α-Fe_2O_3 precursors and magnetic nanomaterials. It is obvious that all particles of α-Fe_2O_3 precursors and Fe_3O_4@C spindles alike have a mean particle (106 nm in diameter and 470 nm in length). Remarkably, there is no significant change in dimension and size of all nanoparticles after Fe_3O_4-core@C-shell composite has formed. The chemical composition of the as-obtained products is further elucidated by SEM with EDS as shown in Fig. 2c. The results indicate that the carbon is successfully coated on Fe_3O_4.

The structure of the as-obtained products is further investigated by X-ray powder diffraction (XRD). Fig. 3 shows the typical XRD pattern of α-Fe_2O_3, in which all peaks unique for α-Fe_2O_3 such as the peaks at 24.13, 33.09, and 40.88° are observed. All the diffraction peaks of α-Fe_2O_3 are in good agreement with α-Fe_2O_3 (JCPDS No. 89-8103). However, the crystal structure of samples has changed dramatically after the α-Fe_2O_3 precursors are reduced to Fe_3O_4 under N_2 atmosphere at 600 °C for 12 h. It is obvious that the unique peaks for Fe_2O_3 disappear completely and new characteristic peaks appear. All diffraction peak positions of Fe_3O_4@C are consistent with face-centered Fe_3O_4 (JCPDS No. 65-3107). It is worth noting that the XRD diffraction peak of graphite are not found in the XRD pattern, indicating the carbon coatings are not well crystallized. Both the morphology and structure are the same as those reported in literature [35].

The VSM is used to evaluate the magnetic properties of Fe_3O_4@C composites, which is shown in Fig. 4. It can be seen from Fig. 4 that the magnetization curve shows the typical hysteresis loops, suggesting that the as-obtained products has ferromagnetic properties. The saturation magnetization (Ms) value of as-obtained is up to 38.9 emu g^{-1}, which is good for us to design a forced convection nanofluids absorption system using external rotating magnetic field and separate the nanoparticles from nanofluids by magnetic separation technique. The typical hysteresis loop is shown in inset of Fig. 4. The result shows that Fe_3O_4@C composites have strong magnetic responsiveness, which provides a possibility for the implementation of a forced convective nanofluids absorption system through an external rotating magnetic field, and separating the nanoparticles from high temperature nanofluids by magnetic separation technology.

3.2. The stability and viscosity of nanofluids

The stability of the nanofluids has great influence on their heat transfer proficiency. Thus, the free settling experiment of nanofluids is carried out as shown in Fig. 5. The results show that the color of the nanofluids change gradually darker and darker with the increase of the concentrations. And no obvious precipitations are found after being stored for 2 weeks, indicating that the Fe_3O_4@C-oil has high stability and reliability.

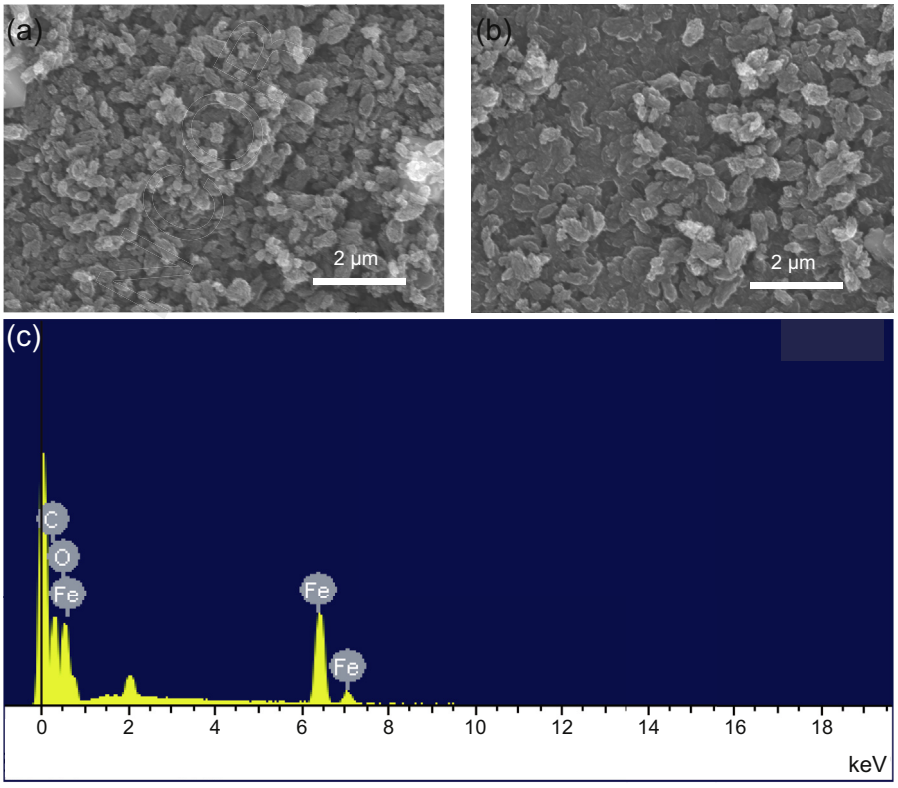

Fig. 2. SEM images of (a) α-Fe_2O_3, (b) Fe_3O_4@C; (c) Energy Dispersive Spectrometer of Fe_3O_4@C.

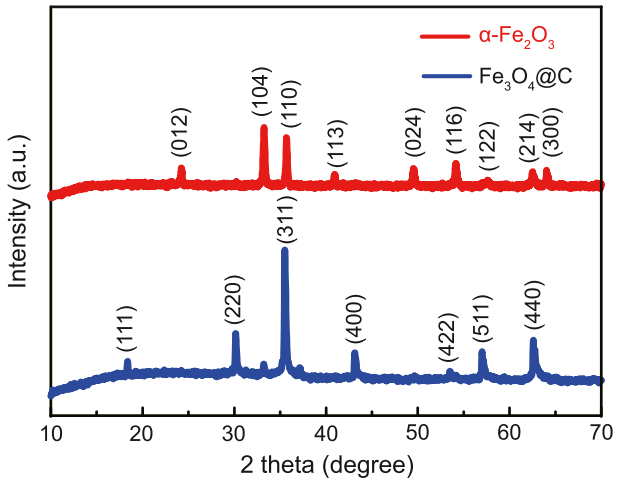

Fig. 3. XRD patterns of α-Fe_2O_3 and Fe_3O_4@C composites.

But as we all know, the nanoparticle agglomerates are unavoidable during long-term using process, which will lead to a series of problems such as plugging of the tube bank of the heat exchanger and the increased flow resistance. This problem can be solved surprise by separating the nanoparticle from high temperature nanofluids via magnetic separation technology before it flows into the heat exchanger, as shown in Fig. 1b.

Viscosity of the nanofluids as a thermophysical parameters has important practical meaning for engineering practice. The effect of adding amount of nanoparticles on the viscosity of base fluid can be clearly seen from the Fig. 6a. The viscosity of all the sample is higher than that of pure oil after adding the Fe_3O_4@C nanoparticles and the viscosity increased nonlinearly with the increase of nanofluid concentration, which is in agreement with the reported in the literature [36]. The relative viscosity (μ_{nf}/μ_{Oil}) of Fe_3O_4@C-oil nanofluids at different temperature is shown in Fig. 6b. The relative viscosity of all fluids increases nonlinearly with temperature and the maximum relative viscosity occurs at 95 °C. The highest viscosity enhancement of 21% when the concentration is 500 ppm at 95 °C. This means that higher pumping power will be required in energy systems.

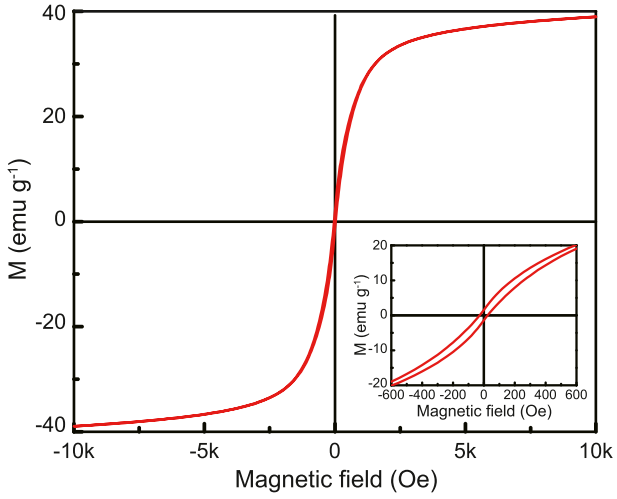

Fig. 4. Magnetization curves of Fe_3O_4@C.

3.3. Optical property of nanofluids

Fig. 7a shows the transmission spectra of Fe_3O_4@C-oil nanofluids with different concentration. It is obvious that the transmittance of all the fluids with different concentrations shows the same change trend as pure base fluid in the whole wavelength range. However, all the nanofluid shows the lower transmittances compared with the base fluid, indicating that the absorption property of fluid can be considerably improved by adding nanoparticles. Specifically, in the visible range, the transmittance decreases from 92% to 1.2% when the concentration of Fe_3O_4@C-oil nanofluids is raised from 0 ppm to 500 ppm.

The extinction coefficient ($K_{e\lambda}$) can be calculated based on the spectral transmittance $T(\lambda)$ of nanofluids by the Lambert–Beer law [37]:

$$T(\lambda) = \exp(-K_{e\lambda} d) \tag{5}$$

where d is the optical path length that is 10 mm in our work. The spectral extinction coefficient is shown in Fig. 7b. Generally, the higher extinction coefficient of fluids, the better the optical absorbance. It can be seen that the extinction coefficient values of all the nanofluids are much higher than that of pure base fluid, revealing that the absorption property of fluid can be greatly improved by dispersing nanoparticles into the fluids.

To directly evaluate the absorbed light by nanofluids, the absorbed solar power spectrum of nanofluids ($S_n(\lambda)$) is obtained by the following equation:

$$S_n(\lambda) = (1 - T(\lambda)) S_{AM1.5} \tag{6}$$

where, $S_{AM1.5}$ represents the solar power spectrum of AM 1.5, which refers to the ASTMG173, Global. It can be observed that the $S_n(\lambda)$ curve of nanofluids is coming closer and closer to the solar irradiance with the increase of concentration of nanofluids. In particular, the $S_n(\lambda)$ curve of nanofluids nearly overlap the spectral solar irradiance when the concentration is 500 ppm as shown in Fig. 7c. The results show that high concentration of nanofluids favors light resource capture and energy conversion.

The absorbed energy fraction, F, a quantitative measurable index to assess the amount of absorbed incident radiation, is calculated by using the following equation [38]:

$$F = \frac{\int_{300}^{1800} I(\lambda)(1 - T(\lambda)) d\lambda}{\int_{300}^{1800} I(\lambda) d\lambda} \tag{7}$$

where $I(\lambda)$ represents the spectral solar irradiance. Fig. 7(d) shows the absorbed energy fraction of nanofluids as a function

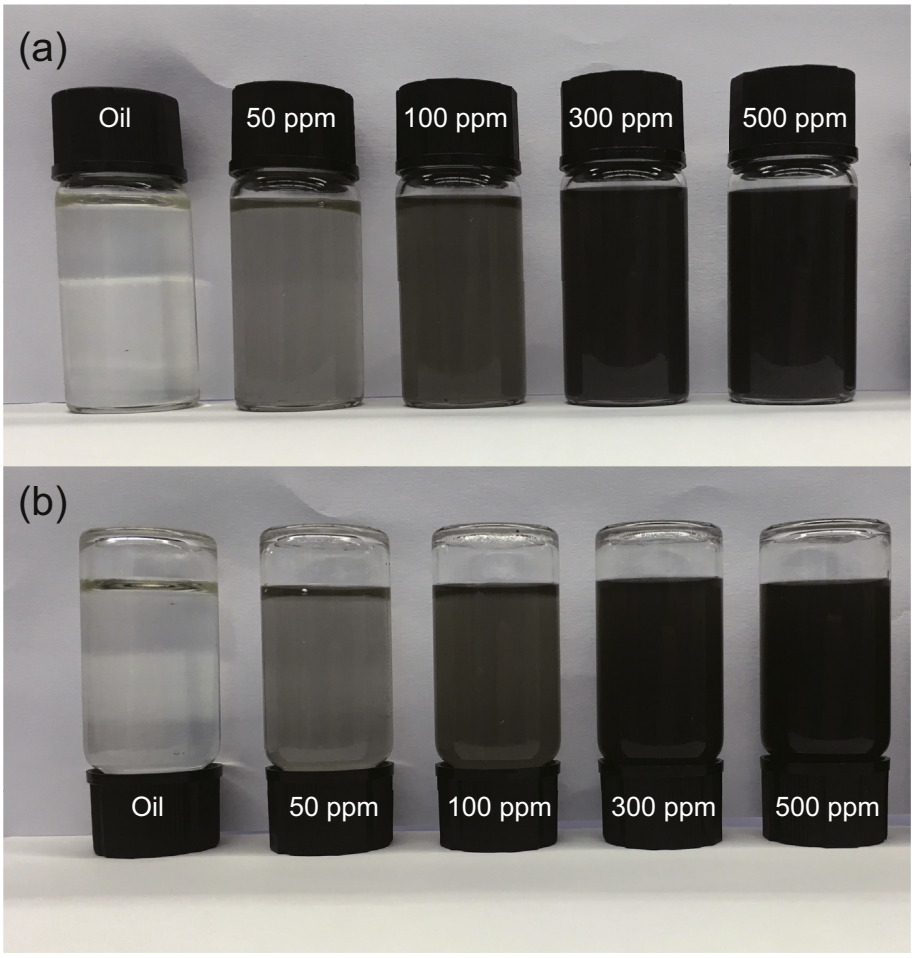

Fig. 5. Photographs of the Fe_3O_4@C-oil nanofluids with different concentrations: (a) fresh prepared and (b) after being stored for 2 weeks.

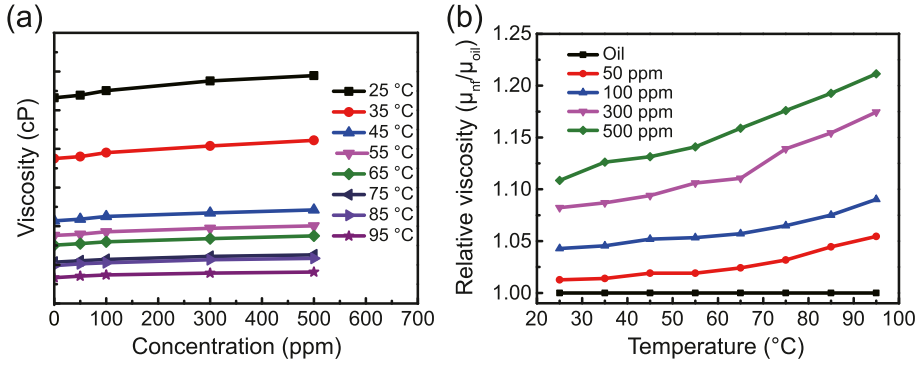

Fig. 6. (a) Viscosity of Fe_3O_4@C-oil nanofluids with different concentrations; (b) Relative viscosity (μ_{nf}/μ_{Oil}) of Fe_3O_4@C-oil nanofluids at different temperature.

of penetration distance. It can be seen that the *F* of all the fluid increases with the penetration depth. Meanwhile, no matter how deep the pure oil is, the *F* cannot be up to 100%. By contrast, the nanofluids is very easy to do this, especially for high concentration. It can also be observed that the *F* has reached up to 100% at the penetration depth only 0.9 cm when the concentration of nanofluids is 500 ppm. It means that all the incident radiation is absorbed at the top area of nanofluids and more energy is lost to the environment in DASCs, which is disadvantage for the practical application.

3.4. Temperature distributions

The temperature rise curves of Oil and Fe_3O_4@C-oil nanofluids with different concentration at the irradiation of 2500 s are shown as in Fig. 8a–c. It can be seen that

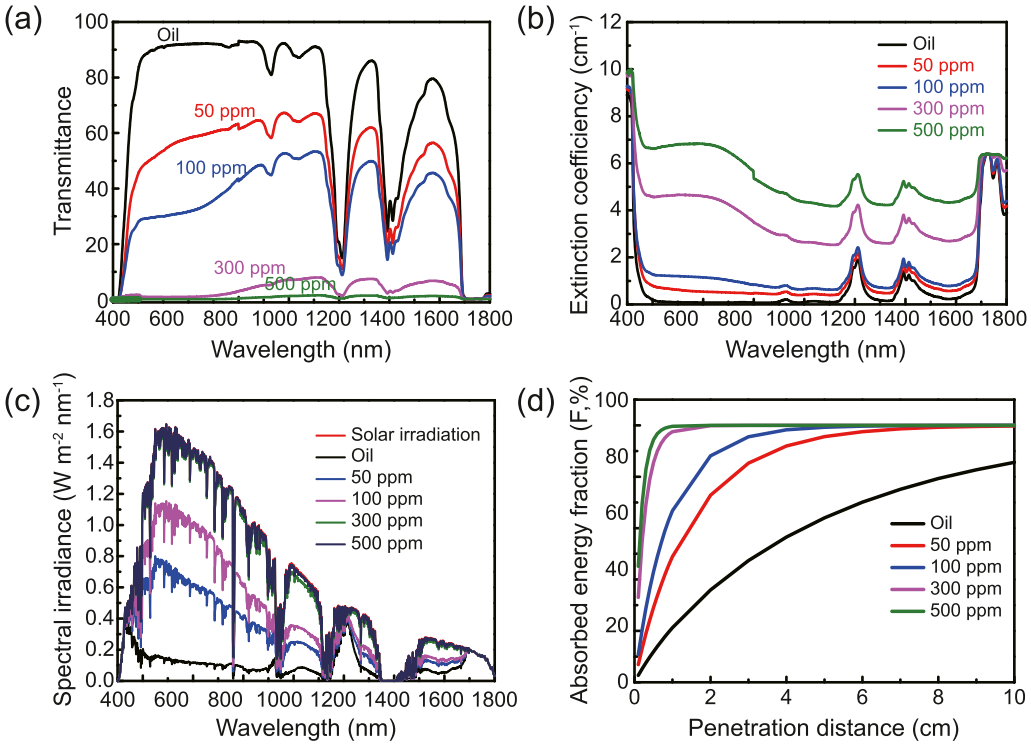

Fig. 7. (a) Transmittance spectra, (b) Extinction coefficient, (c) Spectral irradiance, (d) Absored energy fraction of Fe_3O_4@C-oil nanofluids with different concentration.

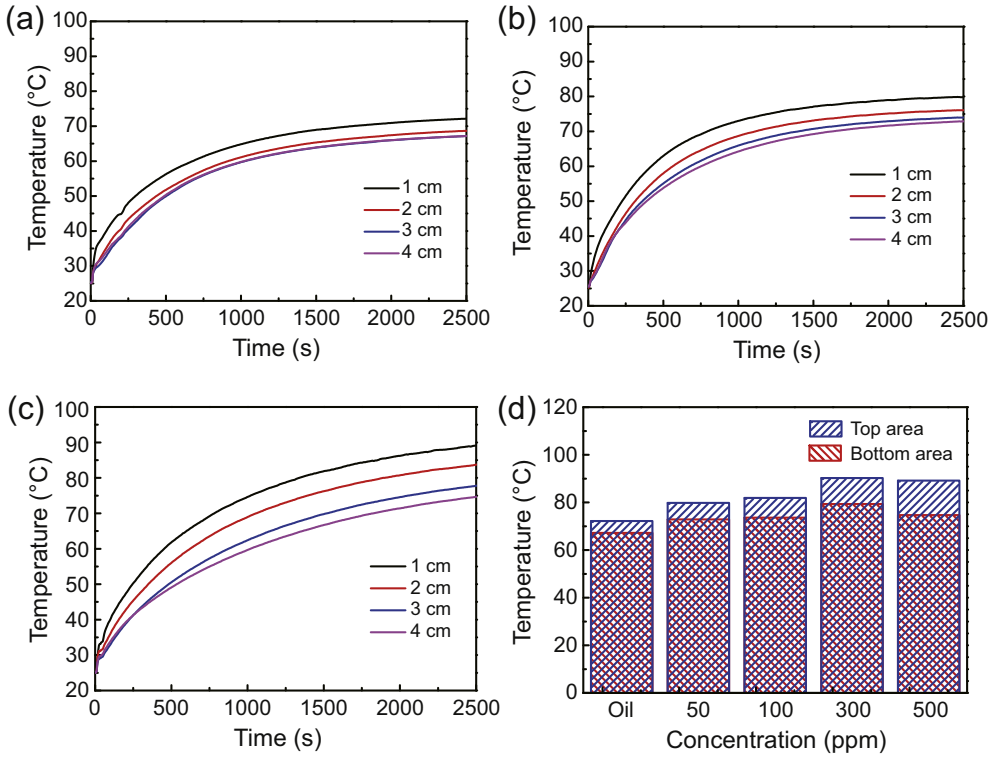

Fig. 8. Temperature rise curves of (a) Oil and Fe_3O_4@C-oil nanofluids with different concentration (b) 50 ppm, (c) 500 ppm and (d) top area and bottom area temperature of nanofluids with different concentration.

temperatures of all fluids increase first and then decrease with the increase of irradiation time. During initial steps, the temperature of all fluids rises rapidly due to the low heat dissipation rate to environment. Then the temperature increasing rate gradually reduces with the temperature difference between the liquids and the environment increasing, and after some time the change of temperature becomes mild. It can be observed from Fig. 8d that the temperature difference between top area and bottom area of nanofluids change from 4.96 °C for pure oil to 14.15 °C for nanofluids with 500 ppm. Meanwhile, the temperature gradient the gaps also has the tendency to expand in this system, particularly for high concentration. In other words, the high concentration nanofluids is unfavorable to the light-thermal conversion of nanofluids. This is mainly because that the vast majority of solar irradiance is absorbed by the top area of nanofluids and converted to heat. Accordingly, the top area of nanofluids becomes the hottest part of the whole system, which has resulted in the large heat loss to environment instead of transferring to the bottom. The other temperature rise curves of nanofluids with different concentrations can be obtained from Figs. S1 and S2.

3.5. Photothermal conversion efficiency

The temperature rise curves of the nanofluids with different concentration are shown in Fig. 9a. It can be seen that temperature rise curve changes from a smooth curve to zigzag after adding the external rotating magnetic field. After the irradiation of 2500 s, the maximum temperature of Fe_3O_4@C-oil nanofluids reach up to 81.91 °C and 98.55 °C when the concentration is 50 ppm and 500 ppm, respectively. Other temperature rise curves of nanofluids with different concentrations at external rotating magnetic field can be obtained from Fig. S3. It can also be observed that temperature of the nanofluids increase greatly under external rotating magnetic field, specially at bottom of nanofluids. The maximum temperature increment is up to 9.1, 5.1, 9.35 and 15.28 °C when the concentration is 50, 100, 300 and 500 ppm, respectively, as shown in Fig. 9c. Correspondingly, compared with no external rotating magnetic field, the total absorbed energy of the whole nanofluids also increased considerably as shown in Fig. 9d. Obviously, under solar light irradiation, the total absorbed energy of nanofluids show the increasing trend with the increasing of the concentration of nanofluids. After 2500 s irradiation, the energy absorption of fluids increases from 1632.2, 1683.8, 1904.6 and 1827.2 J to 1790.7, 1773.7, 2090.4 and 2212.6 J after adding the external rotating magnetic field when the concentration is 50, 100, 300 and 500 ppm, respectively. The total energy absorption curves of Fe_3O_4@C-oil at external rotating magnetic field and non-external rotating magnetic field can be obtained from Fig. S3, which strongly suggests that the interference of external rotating magnetic field can improve the utilization of solar energy.

The photothermal conversion efficiency of pure oil and Fe_3O_4@C-oil nanofluids with different concentration are shown in Fig. 10. It is obvious that all the nanofluids have a higher efficiency than pure oil, indicating that the photothermal conversion efficiency of DASCs can be improved by adding the

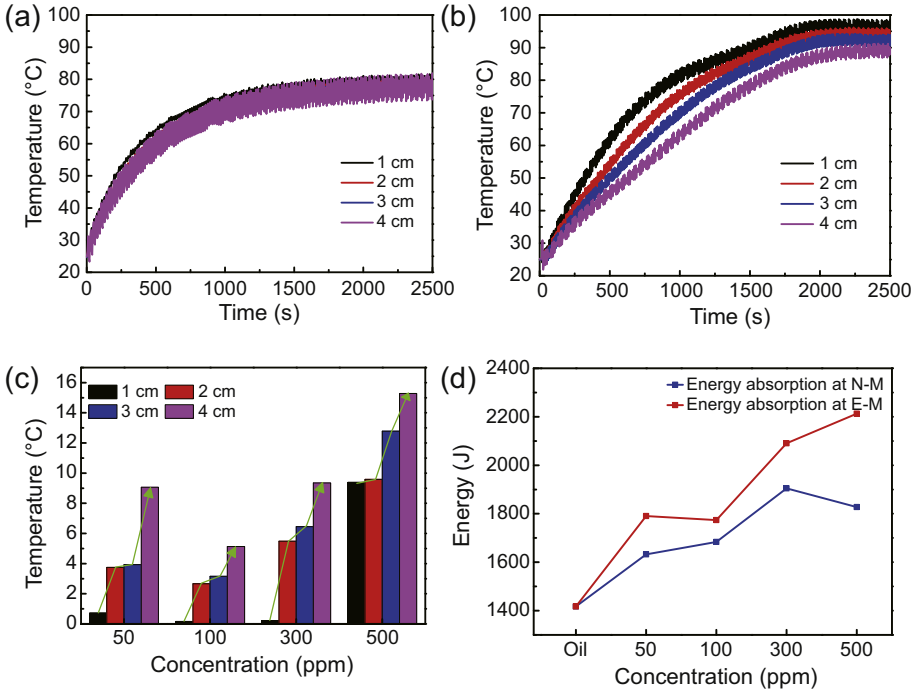

Fig. 9. Temperature rise curves of Fe_3O_4@C-oil nanofluids with different concentration (a) 50 ppm, (b) 500 ppm and (c) temperature increment of each layer, (d) total absorbed energy of the bulk nanofluids with different concentration at external rotating magnetic field and non-external rotating magnetic field (E-M and N-M represent external rotating magnetic field and non-external rotating magnetic field, respectively).

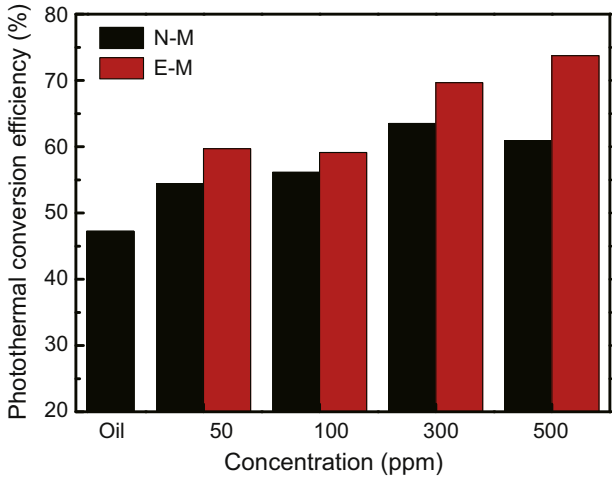

Fig. 10. The photothermal conversion efficiency of Fe_3O_4@C-oil nanofluids with different concentration at 2500 s (E-M and N-M represent external rotating magnetic field and non-external rotating magnetic field, respectively).

nanoparticles into base fluids. It can be noticed that the maximal photothermal conversion efficiency of Fe_3O_4@C-oil nanofluids (300 ppm) is increased up to 34.5% compared with pure oil. It seems that the photothermal conversion ability of nanofluids is positively correlated with the concentration. However, after further increasing the concentration, the photothermal conversion efficiency decreases. This phenomenon is caused by the fact that most of the radiation is only absorbed by the top layer of nanofluids and much of heat loss to environment through the top surface of cuvette [39]. Furthermore, the photothermal conversion efficiency of all the nanofluids can be further improved after adding the external rotating magnetic field. The maximal photothermal conversion efficiency reaches up to 73.7% by increasing the concentration from 0 to 500 ppm under the external rotating magnetic field. Compared with no external rotating magnetic field, the photothermal conversion efficiency of all the nanofluids increases by 9.7%, 5.3%, 9.8% and 21.1% when the concentration is 50, 100, 300 and 500 ppm, respectively. The reason for this phenomenon is that the heat transfer mechanism of working fluids is changed from heat conduction to the thermal convection in DASCs.

4. Conclusions

In this work, a new method of using magnetic nanofluids based on Fe_3O_4@C-oil nanofluids as the working fluids of DASCs is proposed. By this system, not only high-quality energy is got, but also the problems of blockage and corrosion in heat exchanger are well avoided. The main conclusions are as follows:

- The high-quality energy is got. The maximum temperature of DASCs can reach 98 °C by adding Fe_3O_4@C magnetic nanoparticles into pure oil under 3 solar irradiations. The photothermal conversion efficiency is increased from 42.2% to 60.9% with the increasing concentration of nanofluids from 0 to 500 ppm.
- A forced convective nanofluids absorption system is designed to further improve the photothermal conversion efficiency of DASCs by adding an external rotating magnetic field. Compared with no external rotating magnetic field, the photothermal conversion efficiency increased by 12.8% when the concentration is 500 ppm. The main reason is that the heat transfer mechanism of working fluids is changed from heat conduction to the thermal convection, which decrease heat loss to the environment.
- The method not only reduces the flow resistance in pipeline, but also avoids the problems such as blockage and corrosion in heat exchanger. In this method, the Fe_3O_4@C nanoparticles are separated from the high temperature nanofluids by magnetic separation technology. The obtained pure base liquids with high temperature flow to heat exchanger where all kinds of high temperature liquids that we needed can be obtained.

Conflict of interest

The authors declare no conflict of interests.

Acknowledgments

The work was supported by National Natural Science Foundation of China (51590901 & 51876112 & 51906132 & 51906123), Shanghai Municipal Natural Science Foundation (Grant No. 17ZR1411000), the Key Subject of Shanghai Polytechnic University (Material Science and engineering; Grant Nos. XXKZD1601 and EGD18YJ0042).

Appendix A. Supplementary data

Supplementary data to this article can be found online at https://doi.org/10.1016/j.gee.2020.03.014.

References

[1] G. Ye, N.Y. Doumon, S. Rousseva, Y.R. Liu, M. Abdu-Aguye, M.A. Loi, J.C. Hummelen, L.J.A. Koster, R.C. Chiechi, ACS Appl. Energy Mater. 2 (2019) 2197–2204.
[2] S.Y. Lim, C.S. Law, M. Markovic, L.F. Marsal, N.H. Voelcker, A.D. Abell, A. Santos, ACS Appl. Energy Mater. 2 (2019) 1169–1184.
[3] A. Hirano, R. Ueda, S. Hirayama, Y. Ogushi, Energy 22 (1997) 137–142.
[4] Z. Zheng, C. Chao, W.T. Wu, F.F. Wang, L.L. Du, X.Y. Zhang, Y. Xiong, X.W. He, Y.J. Cai, R.T.K. Kwok, J.W.Y. Lam, X.K. Gao, P.C. Sun, D.L. Phillips, D. Ding, B.Z. Tang, Nat. Commun. 10 (2019) 768.
[5] S.A. Lindley, J.Z. Zhang, ACS Appl. Nano Mater. 2 (2019) 1072–1081.
[6] Q.Z. Li, W.L. Hou, F. Peng, H.L. Wang, S. Zhang, D.Y. Dong, S.Y. Wu, H.Q. Zhang, J. Mater. Sci. 54 (2018) 217–227.
[7] J.E. Minardi, H.N. Chuang, Sol. Energy 17 (1975) 179–183.
[8] S.U.S. Choi, J.A. Eastman, Enhancing thermal conductivity of fluids with nanoparticles, United States, 1995. https://www.osti.gov/servlets/purl/196525.
[9] L.F. Chen, H.Q. Xie, Thermochim. Acta 497 (2010) 61–67.

[10] L.L. Wang, G.H. Zhu, M. Wang, W. Yu, J. Zeng, X.X. Yu, H.Q. Xie, Q. Li, Sol. Energy 184 (2019) 240–248.
[11] C.A. Wisut, B. Sridevi, F. Chun, F. Derek, P. Gerrard, Nanomaterials 7 (2017) 131.
[12] H.K. Moon, H.L. Sang, H.C. Choi, ACS Nano 3 (2009) 3707–3713.
[13] L.L. Chen, J. Liu, X.M. Fang, Z.G. Zhang, Sol. Energy Mater. Sol. Cells 163 (2017) 125–133.
[14] S. Ma, K. Chen, Y.H. Qiu, L.L. Gong, G.M. Pan, Y.J. Lin, Z.H. Hao, L. Zhou, Q.Q. Wang, J. Mater. Chem. A 7 (2019) 3408–3414.
[15] D.H. Zhu, G.W. Huang, L.Y. Zhang, Y. He, H.Q. Xie, W. Yu, Energy Environ. Mater. 2 (2019) 22–29.
[16] Z.D. Hood, K.P. Kubelick, K.D. Gilroy, D. Vanderlaan, X. Yang, M.X. Yang, M.F. Chi, S.Y. Emelianov, Y.N. Xia, Nanoscale 11 (2019) 3013–3020.
[17] M. Mehrali, M.K. Ghatkesar, R. Pecnik, Appl. Energy 224 (2018) 103–115.
[18] Y.M. Xuan, Q. Li, W.F. Hu, AIChE J. 49 (2013) 1038–1043.
[19] R. Prasher, P.E. Phelan, P. Bhattacharya, Nano Lett. 6 (2006) 1529–1534.
[20] W. Evans, R. Prasher, J. Fish, P. Meakin, P. Phelan, P. Keblinski, Int. J. Heat Mass Transfer 51 (2018) 1431–1438.
[21] O. Jaber, G.F. Naterer, I. Dincer, Heat Mass Transf. 46 (2010) 999–1012.
[22] X.P. Yang, X.X. Yang, J. Ding, Y.Y. Shao, F.G.F. Qin, R.H. Jiang, Appl. Therm. Eng. 48 (2012) 24–31.
[23] R.W. Bradshaw, J.G. Cordaro, N.P. Siege, ASME 2008 2nd International Conference on Energy Sustainability Collocated with the Heat Transfer, Fluids Engineering, and 3rd Energy Nanotechnology Conferences, American Society of Mechanical Engineers, 2008, pp. 631–637.
[24] Q. Peng, J. Ding, X.L. Wei, J.P. Yang, X.X. Yang, Appl. Energy 87 (2010) 2812–2817.
[25] F. Buttinger, T. Beikircher, M. Pröll, W. Schölkopf, Sol. Energy 84 (2010) 1166–1174.
[26] M. Zhang, L. Ding, J. Zheng, L. B Liu, H. Alsulamic, M.A. Kutbic, J.L. Xu, Appl. Surf. Sci. 509 (2020) 145348.
[27] M. Zhang, J. Zheng, J.P. Wang, J.L. Xu, T. Hayat, N.S. Alharbid, Sens. Actuators B Chem. 282 (2019) 85–95.
[28] M. Zhang, T. Miao, J. Zheng, J.L. Xu, A.M. Asiri, H.M. Marwani, Micropor. Mesopor. Mater. 286 (2019) 207–213.
[29] D.B. Wang, Y.L. Jia, Y. He, L.L. Wang, H.Q. Xie, W. Yu, Energy Convers. Manag. 199 (2019) 111996,
[30] D.B. Wang, Y.L. Jia, Y. He, L.L. Wang, H.Q. Xie, W. Yu, J. Colloid Interface Sci. 557 (2019) 266–275.
[31] C. Zeng, W. Weng, T. Lv, W. Xiao, ACS Appl. Mater. Interfaces 10 (2018) 30470–30478.
[32] W.M. Zhang, X.L. Wu, J.S. Hu, Y.G. Guo, L.J. Wan, Adv. Funct. Mater. 18 (2010) 3941–3946.
[33] M. Amjad, G. Raza, Y. Xin, S. Pervaiz, J.L. Xu, X.Z. Du, D.S. Wen, Appl. Energy 206 (2017) 393–400.
[34] R.J. Moffat, J. Fluids Eng. 107 (1985) 173–178.
[35] M. Ozaki, S. Kratohvil, E. Matijević, J. Colloid Interface Sci. 102 (1984) 146–151.
[36] S.K. Das, N. Putra, W. Roetzel, Int. J. Heat Mass Transfer 46 (2003) 851–862.
[37] M.J. Chen, Y.R. He, J. Huang, J.Q. Zhu, Int. J. Heat Mass Transfer 108 (Part B) (2017) 1894–1900.
[38] W.D. Drotning, Sol. Energy 20 (1978) 313–319.
[39] J. Zeng, Y.M. Xuan, Appl. Energy 212 (2018) 809–819.